Supporting Information

Tungsten(VI)-Copper(I)-Sulfur Cluster-Supported Metal-Organic Frameworks Bridged by *in Situ* Click-Formed Tetrazolate Ligands

Qiu-Fang Chen,[†,‡] Xin Zhao,[†] Quan Liu,[†] Ji-Dong Jia,[§] Xiao-Ting Qiu,[†] Ying-Lin Song,[§] David James Young,[¶] Wen-Hua Zhang,[*,†] and Jian-Ping Lang[*,†,‡]

[†]State and Local Joint Engineering Laboratory for Novel Functional Polymeric Materials, College of Chemistry, Chemical Engineering and Materials Science, Soochow University, Suzhou 215123, Jiangsu, P. R. China

[‡]State Key Laboratory of Organometallic Chemistry, Shanghai Institute of Organic Chemistry, Chinese Academy of Sciences, Shanghai 200032, P. R. China

[§]School of Physical Science and Technology, Soochow University, Suzhou 215006, Jiangsu, P. R. China

[¶]Faculty of Science, Health, Education and Engineering, University of the Sunshine Coast, Maroochydore, Queensland 4558, Australia

---

To whom correspondence should be addressed. E-mail: jplang@suda.edu.cn & whzhang@suda.edu.cn

† Soochow University

‡ Shanghai Institute of Organic Chemistry

§ Soochow University

¶ University of the Sunshine Coast

Contents

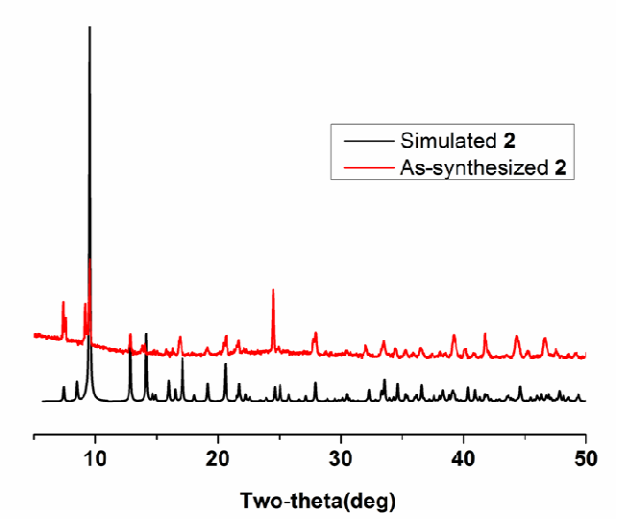
Simulated 2
As-synthesized 2
10
20
30
40
50
Two-theta(deg)

(a)

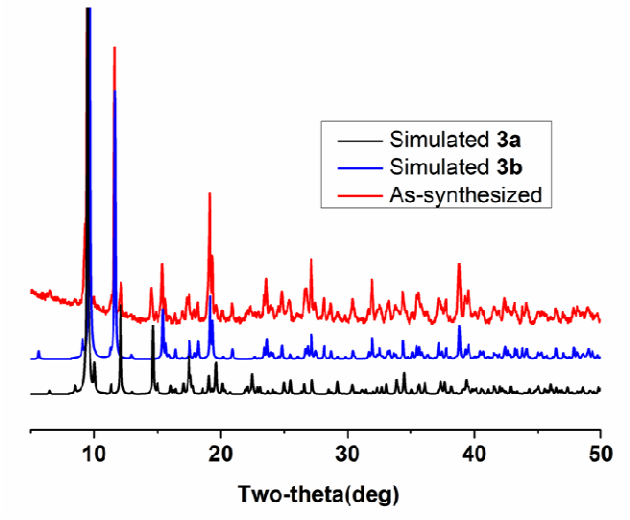
Simulated 3a
Simulated 3b
As-synthesized
10
20
30
40
50
Two-theta(deg)

(b)

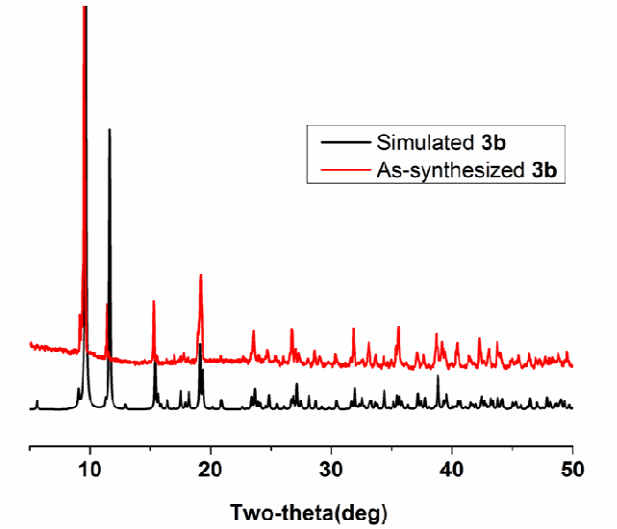
Simulated 3b
As-synthesized 3b
10
20
30
40
50
Two-theta(deg)

(c)

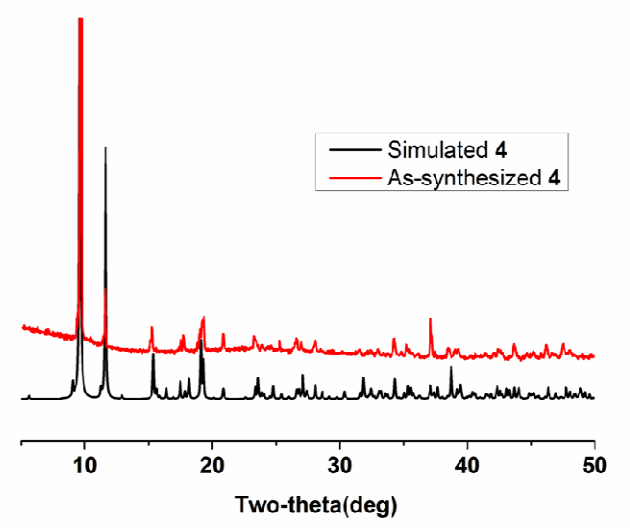
Simulated 4
As-synthesized 4
10
20
30
40
50
Two-theta(deg)

(d)

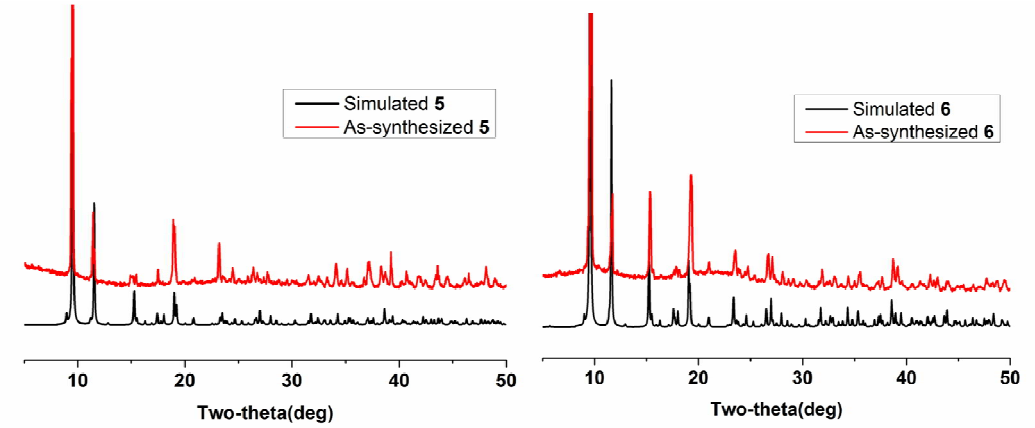

(e) (f)

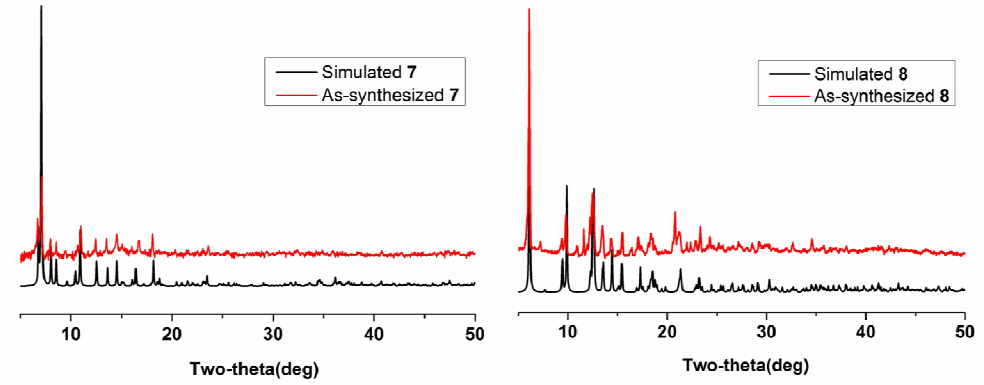

(g) (h)

Figure S1. (a) PXRD patterns of **2**. Simulated (black), single-phase polycrystalline sample (red). (b) PXRD patterns of **3a** accompanied by the presence of **3b**. Simulated (**3a**, black; **3b**, blue), single-phase polycrystalline sample (red). (c) PXRD patterns of **3b**. Simulated (black), single-phase polycrystalline sample (red). (d) PXRD patterns of **4**. Simulated (black), single-phase polycrystalline sample (red). (e) PXRD patterns of **5**. Simulated (black), single-phase polycrystalline sample (red). (f) PXRD patterns of **6**. Simulated (black), single-phase polycrystalline sample (red). (g) PXRD patterns of **7**. Simulated (black), single-phase polycrystalline sample (red). (h) PXRD patterns of **8**. Simulated (black), single-phase polycrystalline sample (red).

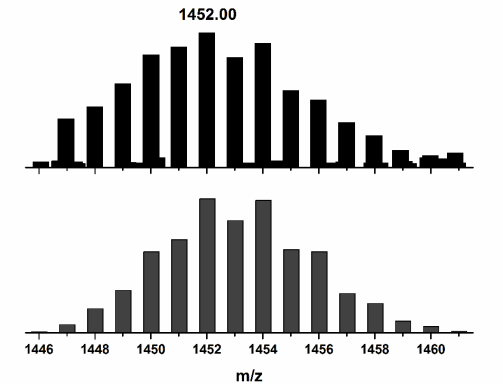

Figure S2. The positive-ion ESI-MS patterns (top) and the calculated isotope patterns (below) of the $\{[(Tp^*WS_3Cu_3)(Btta)_3Cu_2Na]+BF_4+CH_3OH+CH_3CN\}^+$ cation in **5**.

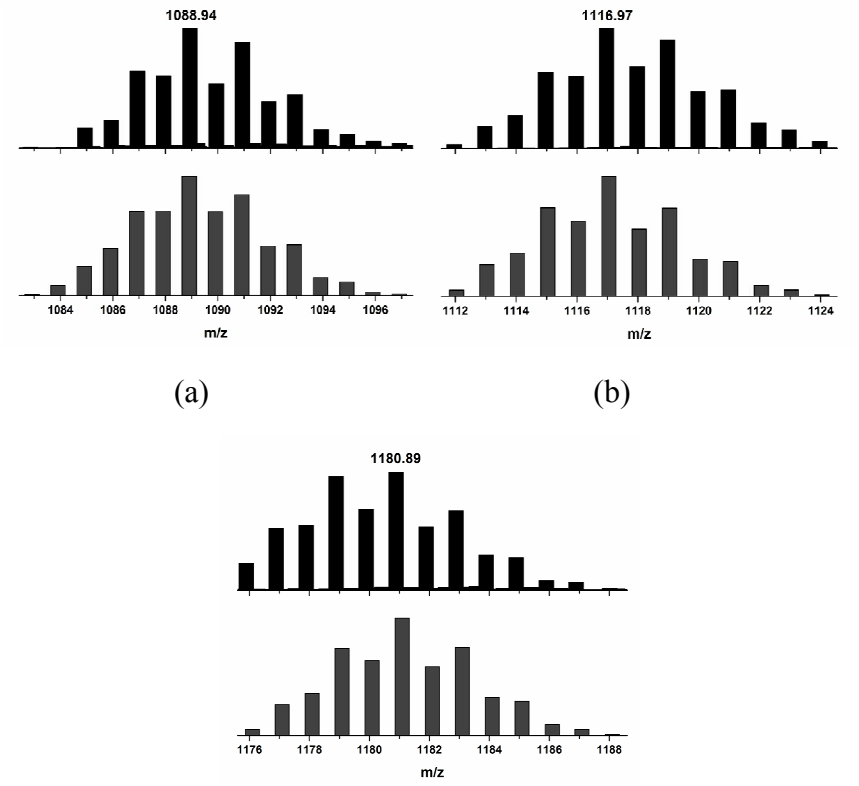

Figure S3. The positive-ion ESI-MS patterns (top) and the calculated isotope patterns (below) of the $\{[(Tp^*WS_3Cu_3)(Petta)Cu]+BF_4+CH_3OH\}^+$ (a), $\{[(Tp^*WS_3Cu_3)(Petta)_2K]+CH_3OH\}^+$ (b) and $\{[(Tp^*WS_3Cu_3)(Petta)_2K]+3CH_3OH\}^+$ (c) cations in **6**.

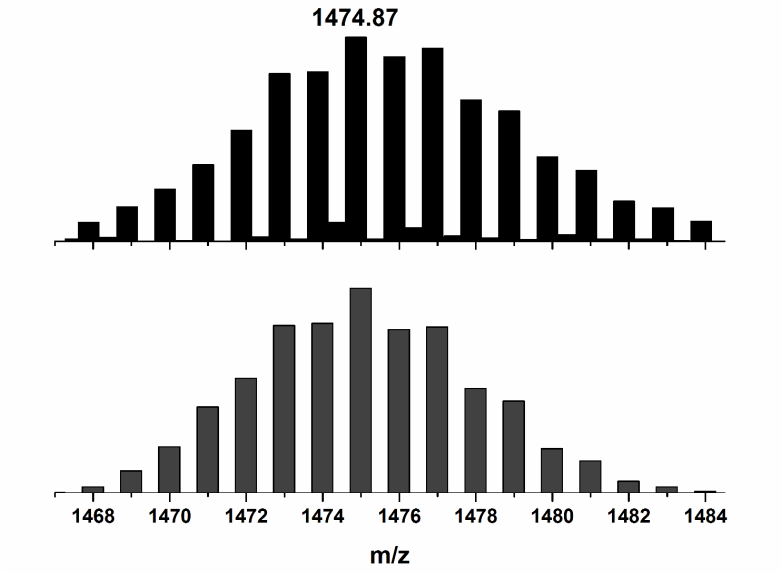

Figure S4. The positive-ion ESI-MS patterns (top) and the calculated isotope patterns (below) of the $\{[(Tp^*WS_3Cu)(Tp^*WS_3Cu_2)(S')]+2H+3CH_3OH\}^+$ cation in **7**.

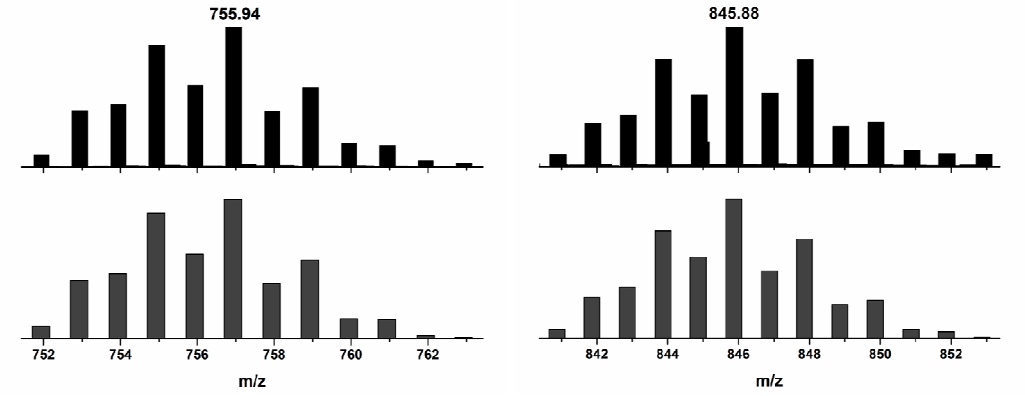

(a) (b)

Figure S5. The negative-ion ESI-MS patterns (top) and the calculated isotope patterns (below) of the $[(Tp^*WS_3Cu_2)(CN)_2]^-$ (a) and $[(Tp^*WS_3Cu_3)(CN)_3]^-$ (b) anions in **8**.

Table S1. Selected Bond Lengths (Å) for 2−8

Compound **2**[a]					
W(1)···Cu(1)	2.6384(5)	W(1)···Cu(1)#1	2.6384(5)	W(1)···Cu(1)#2	2.6384(5)
Cu(1)···Cu(1)#1	2.9291(9)	Cu(1)···Cu(1)#2	2.9291(9)	Cu(1)-S(1)	2.2062(11)
Cu(1)-S(1)#1	2.2099(11)	S(1)-Cu(1)#2	2.2100(11)	Cu(1)-N(3)	1.919(3)
Compound **3a**[b]					
W(1)···Cu(1)	2.625(2)	W(1)···Cu(1)#1	2.625(2)	W(1)···Cu(1)#2	2.625(2)
Cu(1)···Cu(1)#1	2.879(4)	Cu(1)···Cu(1)#2	2.879(4)	Cu(1)-S(1)	2.193(6)
Cu(1)-S(1) #1	2.192(6)	S(1)-Cu(1)#2	2.192(6)	Cu(1)-N(3)	1.921(16)
W(2)···Cu(2)	2.648(2)	W(2)···Cu(2) #1	2.648(2)	W(2)···Cu(2)#2	2.648(2)
Cu(2)···Cu(2)#1	2.857(5)	Cu(2)···Cu(2)#2	2.857(5)	Cu(2)-S(2)	2.228(5)
Cu(2)-S(2)#1	2.214(6)	S(2)-Cu(2)#2	2.214(6)	Cu(2)-N(6)	1.933(16)
Compound **3b**[c]					
W(1)···Cu(1)	2.6325(5)	W(1)···Cu(1)#1	2.6323(5)	W(1)···Cu(1)#2	2.6323(5)
Cu(1)···Cu(1)#1	2.8919(9)	Cu(1)···Cu(1)#2	2.8919(10)	Cu(1)-S(1)	2.2012(12)
S(1)-Cu(1)#1	2.2043(12)	Cu(1)-S(1)#2	2.2045(12)	Cu(1)-N(1)	1.908(4)
Compound **4**[d]					
W(1)···Cu(1)	2.6278(8)	W(1)···Cu(1)#1	2.6278(8)	W(1)···Cu(1)#2	2.6278(8)
Cu(1)···Cu(1)#1	2.8997(14)	Cu(1)···Cu(1)#2	2.8997(14)	Cu(1)-S(1)	2.2088(17)
Cu(1)-S(1)#1	2.1952(17)	S(1)-Cu(1)#2	2.1950(17)	Cu(1)-N(3)	1.901(6)
Compound **5**[a]					
W(1)···Cu(1)	2.6283(7)	W(1)···Cu(1)#1	2.6285(7)	W(1)···Cu(1)#2	2.6285(7)
Cu(1)···Cu(1)#1	2.8982(14)	Cu(1)···Cu(1)#2	2.8983(13)	Cu(1)-S(1)	2.1955(16)
Cu(1)-S(1)#1	2.2002(16)	S(1)-Cu(1)#2	2.2004(15)	Cu(1)-N(1)	1.894(6)
Compound **6**[b]					
W(1)···Cu(1)	2.6299(7)	W(1)···Cu(1)#1	2.6300(7)	W(1)···Cu(1)#2	2.6300(7)
Cu(1)···Cu(1)#1	2.8898(13)	Cu(1)···Cu(1)#2	2.8898(13)	Cu(1)-S(1)	2.1931(16)
Cu(1)-S(1)#2	2.2049(16)	S(1)-Cu(1)#1	2.2046(16)	Cu(1)-N(1)	1.902(5)
Compound **7**[e]					
W(1)···Cu(1)	2.6637(18)	W(1)···Cu(2)	2.6680(15)	W(1)···Cu(3)	2.6762(18)
Cu(1)···Cu(2)	2.8642(16)	Cu(1)···Cu(3)	2.916(2)	Cu(2)···Cu(3)	2.8936(16)
Cu(1)-S(1)	2.2197(19)	Cu(1)-S(2)	2.229(2)	Cu(1)-S(4)	2.187(2)
Cu(2)-S(2)	2.218(2)	Cu(2)-S(3)	2.224(2)	Cu(2)-S(4)#1	2.1833(19)
Cu(3)-S(1)	2.2280(19)	Cu(3)-S(3)	2.214(2)	Cu(3)-S(4)#2	2.190(2)
S(4)-Cu(2)#3	2.1833(19)	S(4)-Cu(3)#2	2.190(2)		
Compound **8**[f]					
W(1)···Cu(1)	2.6721(13)	W(1)···Cu(2)	2.6548(15)	W(1)···Cu(3)	2.6539(14)
Cu(1)···Cu(2)	2.954(2)	Cu(1)···Cu(3)	2.9635(19)	Cu(2)···Cu(3)	2.9940(17)
Cu(1)-S(1)	2.237(3)	Cu(1)-S(2)	2.213(3)	Cu(1)-C(1)	1.899(9)
Cu(2)-S(2)	2.220(3)	Cu(2)-S(3)	2.225(3)	Cu(2)-C(5)#1	1.885(9)
Cu(3)-S(1)	2.214(3)	Cu(3)-S(3)	2.204(3)	Cu(3)-C(4)#2	1.898(9)
Cu(4)-C(2)	1.911(7)	Cu(4)-C(3)	1.869(8)	Cu(4)-N(1)	1.942(9)
Cu(5)-N(3)	1.923(9)	Cu(5)-N(4)	1.939(8)	Cu(5)-N(5)	1.942(9)

[a]Symmetry codes for **2** and **5**: #1, –*y* + 2, *x* − *y* + 1, *z*; #2, –*x* + *y* + 1, −*x* + 2, *z*. [b]Symmetry codes for **3a** and **6**: #1, –*y* + 1, *x* −*y* + 2, *z*; #2, –*x* + *y* −1, −*x* + 1, *z*. [c]Symmetry codes for **3b**: #1, –*x* +*y* + 1, −*x* + 1, *z*; #2, –*y* + 1, *x* − *y*, *z*. [d]Symmetry codes for **4**: #1, –*y* + 1, *x* − *y* + 1, *z*; #2, –*x* + *y*, −*x* + 1, *z*. [e]Symmetry codes for **7**: #1, *y* + 1/4, − *x* + 3/4, *z*; #2, –*x* + 1, −*y* + 1/2, *z*; #3, − *y* + 3/4, *x* − 1/4, −*z* +1/4. [f]Symmetry codes for **8**: #1, –*x*, –*y* + 1, *z*; #2, –*x* +1, −*y* + 1, −*z*.

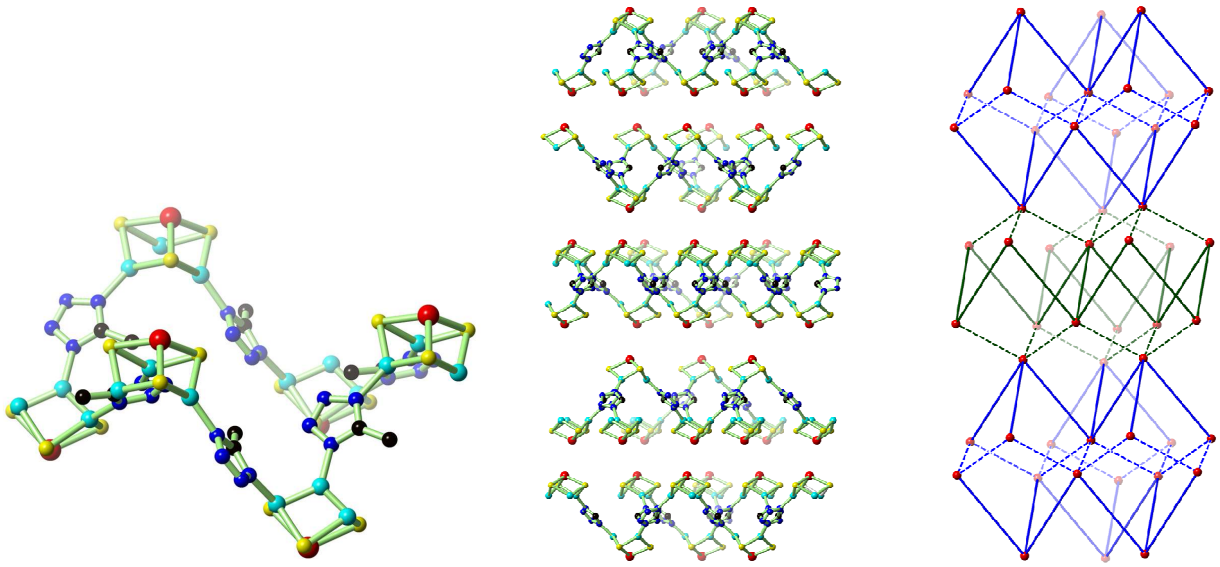

(a) (b) (c)

Figure S6. (a) View of a cyclohexane-shaped $\{[Tp^*WS_3Cu_3]_6(Mtta)_6(\mu_3\text{-}N_3)_3\}^{3+}$ unit in a chair conformation. All Tp* groups, μ_3-N_3 groups, methyl groups and hydrogen atoms are omitted for clarity. (b) The cell packing diagram of **2**. (c) A simplified representation of (b). The solid lines represent 2D layers, and the dotted lines represent the packing between layers. The blue units are the "Type I" spaces, and the green units are the "Type II" spaces.

Table S2. The Variation Data of α, L and R in "Type I" Spaces for **2**−**6**

	2	**3a**	**3b**	**4**	**5**	**6**
α (deg)	134.3	130.4	124	123.8	125.1	126.6
L (Å)	20.107	20.594/ 23.737	24.493	24.542	24.472	24.336
R (Å)	7.220	6.980	6.634	6.650	6.656	6.715

Table S3. The Variation Data of α, L' and R in "Type II" Spaces for **2**−**6**

	2	**3a**	**3b**	**4**	**5**	**6**
α (deg)	134.3	130.4	124	123.8	125.1	126.6
L' (Å)	15.546	18.712	22.479	22.525	22.474	22.256
R (Å)	7.220	6.980	6.634	6.650	6.656	6.715

L' is the W···W separation of the two W atom overlapped along the c direction (polar axis) in "Type II".

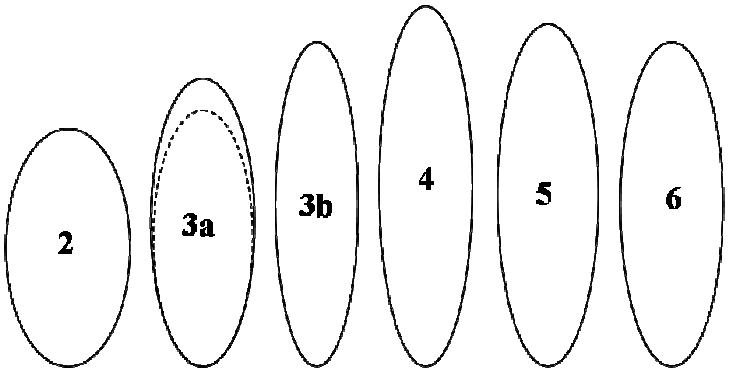

Figure S7. The regular variation diagram of "Type I" spaces for **2**−**6**.

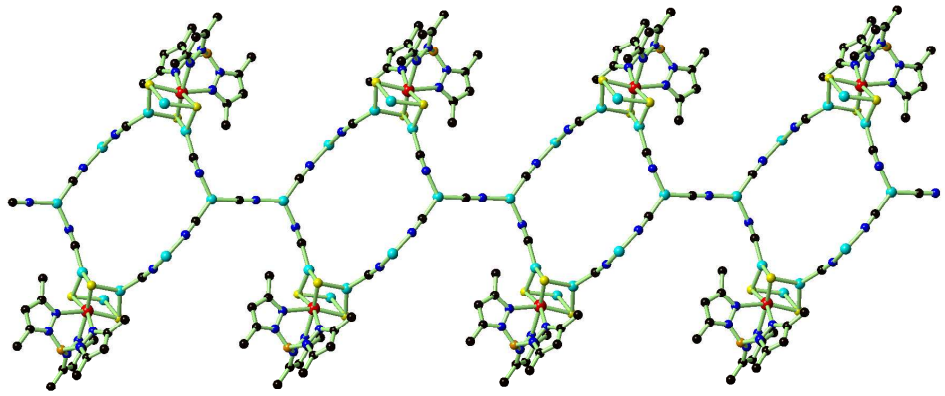

Figure S8. The $\{(Tp^*WS_3Cu_3)[Cu_2(CN)_5]\}_2^{2-}$ unit propagates along the *b* direction through the CN linkage to yield a 1D chain.

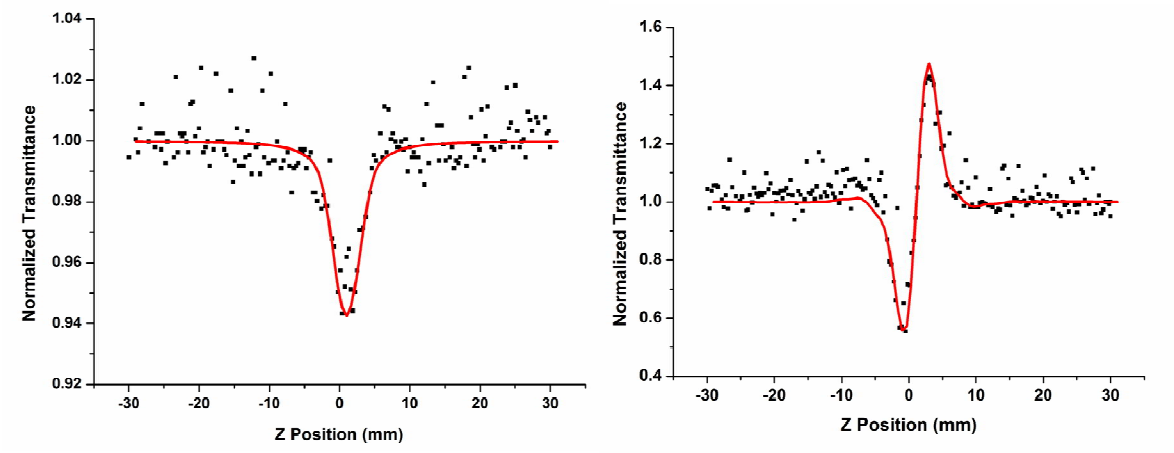

(a) (b)

Figure S9. *Z*-scan data for **6** (5×10^{-5} M) in DMF solution investigated at 532 nm. (a) Normalized *Z*-scan data obtained under the open-aperture configuration showing the nonlinear absorption; (b) collected by dividing the normalized *Z*-scan data under closed-aperture configuration by that in (a) showing the nonlinear refraction. The black solid spheres are experimental data, and the red solid curves are the theoretical fit.

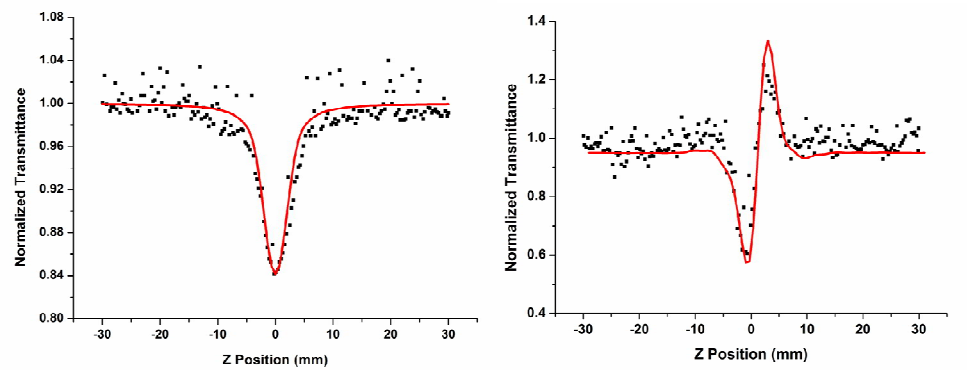

(a) (b)

Figure S10. *Z*-scan data for **7** (5×10^{-5} M) in DMF solution investigated at 532 nm. (a) Normalized *Z*-scan data obtained under the open-aperture configuration showing the nonlinear absorption; (b) collected by dividing the normalized *Z*-scan data under closed-aperture configuration by that in (a) showing the nonlinear refraction. The black solid spheres are experimental data, and the red solid curves are the theoretical fit.

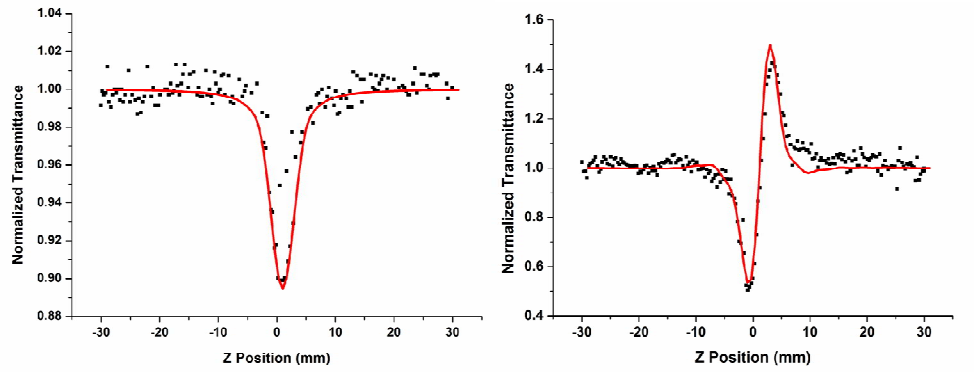

(a) (b)

Figure S11. *Z*-scan data for **8** (5×10^{-5} M) in DMF solution investigated at 532 nm. (a) Normalized *Z*-scan data obtained under the open-aperture configuration showing the nonlinear absorption; (b) collected by dividing the normalized *Z*-scan data under closed-aperture configuration by that in (a) showing the nonlinear refraction. The black solid spheres are experimental data, and the red solid curves are the theoretical fit.

Table S4. The Hyperpolarizability Values (γ) of Some Reported Mo(W)-Cu-S Clusters and Known NLO Active Materials

Compound	γ (esu)	Ref.
1	1.07×10^{-32}	70
C_{60}	7.50×10^{-34}	88
C_{70}	1.30×10^{-33}	88
$[WOS_3Cu_2(4\text{-}^t BuPy)_2]_2$	4.80×10^{-30}	83
$\{[Et_4N]_2[MoOS_3Cu_2(CN)]_2 \cdot 2aniline\}_n$	6.78×10^{-29}	49
$\{[Et_4N]_2[MoOS_3Cu_3(CN)_3]\}_n$	2.47×10^{-28}	49
$\{[Bu_4N][WS_4Cu_3(CN)_2]\}_n$	3.40×10^{-30}	84
$[Cp^*Mo_2S_4Cu_2(dppe)]_2(ClO_4)_4$	6.99×10^{-29}	85
$[Cp^*MoS_3Cu_3(pyz)(NCS)_2]_n$	2.99×10^{-29}	86
$[(Cp^*MoS_3Cu_3)_2(bpea)_3Br_4]_n$	4.00×10^{-29}	53
$[(Cp^*)_2Mo_2S_4(CuI)_2]$	1.18×10^{-29}	87
$\{[Et_4N][Tp^*WS_3(CuSCN)_3(Cu\text{-}\mu_3\text{-}NCS)]\}_n$	4.60×10^{-32}	68
$[Tp^*W(\mu_3\text{-}S)(\mu\text{-}S)_2Cu_2(SCN)(bpp)]_2$	4.80×10^{-32}	67
$[(Tp^*WS_3Cu_2Cl)_2(dppe)]$	4.71×10^{-30}	57
$[(Tp^*WS_3Cu_2Cl)_2(dppbS_2)] \cdot 2MeCN \cdot 2H_2O$	6.13×10^{-30}	57
$[Tp^*WS_3Cu_2(CN)_2Cu(\mu\text{-}py)_2]_2 \cdot 3py$	7.07×10^{-30}	59
$[Tp^*WS_3Cu_2(CN)(\mu_6\text{-}tpt)_{1/3}]_2$	6.32×10^{-30}	59